A study on the effects of laser shock peening on the microstructure and substructure of Ti–6Al–4V manufactured by Selective Laser Melting

J.R.O. Leo [a,b,*], S. Zabeen [a], M.E. Fitzpatrick [a], J. Zou [c], M.M. Attallah [c]

[a] Centre for Manufacturing & Materials Engineering, Coventry University, Coventry CV1 5FB, UK
[b] Materials Engineering, The Open University, Walton Hall, Milton Keynes MK7 6AA, UK
[c] School of Metallurgy and Materials, University of Birmingham, Edgbaston, Birmingham B15 2TT, UK

ARTICLE INFO

ABSTRACT

Ti-6Al-4V was fabricated by powder-bed fusion using different laser scanning strategies. The microstructure and deformation properties were investigated in the as-built condition, and also after the material had been subjected to a laser-shock-peening (LSP) treatment. The microstructure in each condition was surveyed using 3D optical microscopy, EBSD, and TEM. The post-manufacture residual stresses were determined. The results indicate a correlation between the residual stresses and the substructures observed in TEM: tensile residual stresses from the surface down to 1 mm depth were observed in the as-built material, corresponding to extensive deformation through twinning of the $\{10\overline{1}2\}$ type and wavy slip structures; while after LSP the alloy showed a variety of dislocation arrangements, especially planar and in significantly higher density, along with $\{11\overline{2}2\}$ twins and with the presence of compressive residual stresses. The findings indicate that the deformation capability is mechanistically aided by the peening process, which effectively promotes the replacement of tensile residual stresses by compressive ones, offering routes for potentially improving the mechanical properties of the additively manufactured Ti-6Al-4V, as well as its usability.

1. Introduction

Ti-6Al-4V is a dual-phase titanium alloy (α-hcp and β-bcc) with broad application in aerospace, energy, chemical (Bhadeshia, n.d.), marine and biomedical sectors (Liu and Shin, 2019), amongst others. Besides superior biocompatibility (Krakhmalev et al., 2016), the alloy presents desirable mechanical properties: high mechanical strength and toughness, high corrosion resistance, and low density (Boyer, 1996).

However, despite the high level of demand for its commercial use, the undesirable properties of Ti-6Al-4V – namely, its low thermal conductivity, its high reactivity to oxygen at high temperatures, the limited slip systems available owing to its hcp crystal structure, as well as its tendency to strain harden – impose challenges to the manufacturing of its products (Parry et al., 2016). Hence additive manufacturing is of significant current interest to provide alternative fabrication routes, based on cost-effective processes, capability of producing near-net-shaped structures with complex geometries directly from CAD models, and with minimal material waste.

One such process, belonging to the powder-bed fusion route, is Selective Laser Melting (SLM), in which a laser beam scans and melts the feedstock powders, building layer upon layer of molten material that very rapidly cools and solidifies, thus prototyping the desired product (Thijs et al., 2010). Because this process involves rapid melting and resolidification, given the extremely localised heat input and brief interaction time, the microstructure of the Ti-6Al-4V forms under very high cooling rates, reported to reach about 10^6 K/s (Krakhmalev et al., 2016), and severe temperature gradients. This unique thermal history drastically affects the microstructure, promoting the formation of a much less ductile martensitic α'–phase from the β–titanium than that achieved in conventional processing (Kasperovich and Hausmann, 2015), and inducing the development of high-magnitude tensile residual stresses, thus impairing the usability and the mechanical behaviour of the products (Guo et al., 2018).

In order to relieve the surface stresses of the as-built material and so minimise the possibility of distortion, post-processing treatments are used. While heat and thermomechanical treatments may be considered (Vrancken et al., 2012), some fabrication limitations would not be fully addressed (Qiu et al., 2013). Thermomechanical treatments could lead

---

to undesirable geometric deviations in as-built products with complex shapes, and concerns regarding heat treatment causing non-uniformity of the microstructure in parts with irregular shape (Liu and Shin, 2019). Thus, laser shock peening (LSP) offers an alternative process to modify the as-built material surface properties and, with this, improve the mechanical response of the manufactured parts.

LSP is a well-established technique capable of inducing high-magnitude compressive residual stresses at large depths (of the order of millimetres), completely replacing the SLM-generated tensile residual stresses and refining the microstructure to a nanometric grain scale (Nie et al., 2014). Krakhmalev et al. (2016) attributed these effects to the plastic-deformation-induced twinning experienced by the material under the high strain-rates achieved during LSP, while Murr et al. (2009) pointed to the generation, movement and evolution of dislocations as the chief mechanism, and Ren et al. (2016) suggested that both twinning and dislocation motion promote the refinement of the microstructure, but each at a different stage.

The aim of this work was to conduct a comprehensive examination of the Ti-6Al-4V in as-built and LSP conditions, for investigating deformation processes down to the sub-grain scale using both qualitative and quantitative methods. Recent investigations on alloys manufactured by SLM have aimed at surveying and comparing the microstructure and substructure of the as-built material and its LSP-processed counterpart. For example, Kalentics et al. (2019) applied EBSD to SLMed 316 L stainless steel, in order to analyse changes in the microstructure due to LSP. Lu et al. (2020) produced a descriptive TEM survey of substructural features (twins and dislocations) in SLM-LSPed Ti6Al4V; and Lan et al. (2020) provided a qualitative appraisal on the number of such defects in the microstructures of SLMed Ti6Al4V before and after LSP. The present work aligns itself with such studies, by identifying the nature of substructural defects and their evolution throughout the processing of the alloy. Furthermore, accounts of the presence of twins in the post-LSP microstructure vary and are therefore a key element in the investigation.
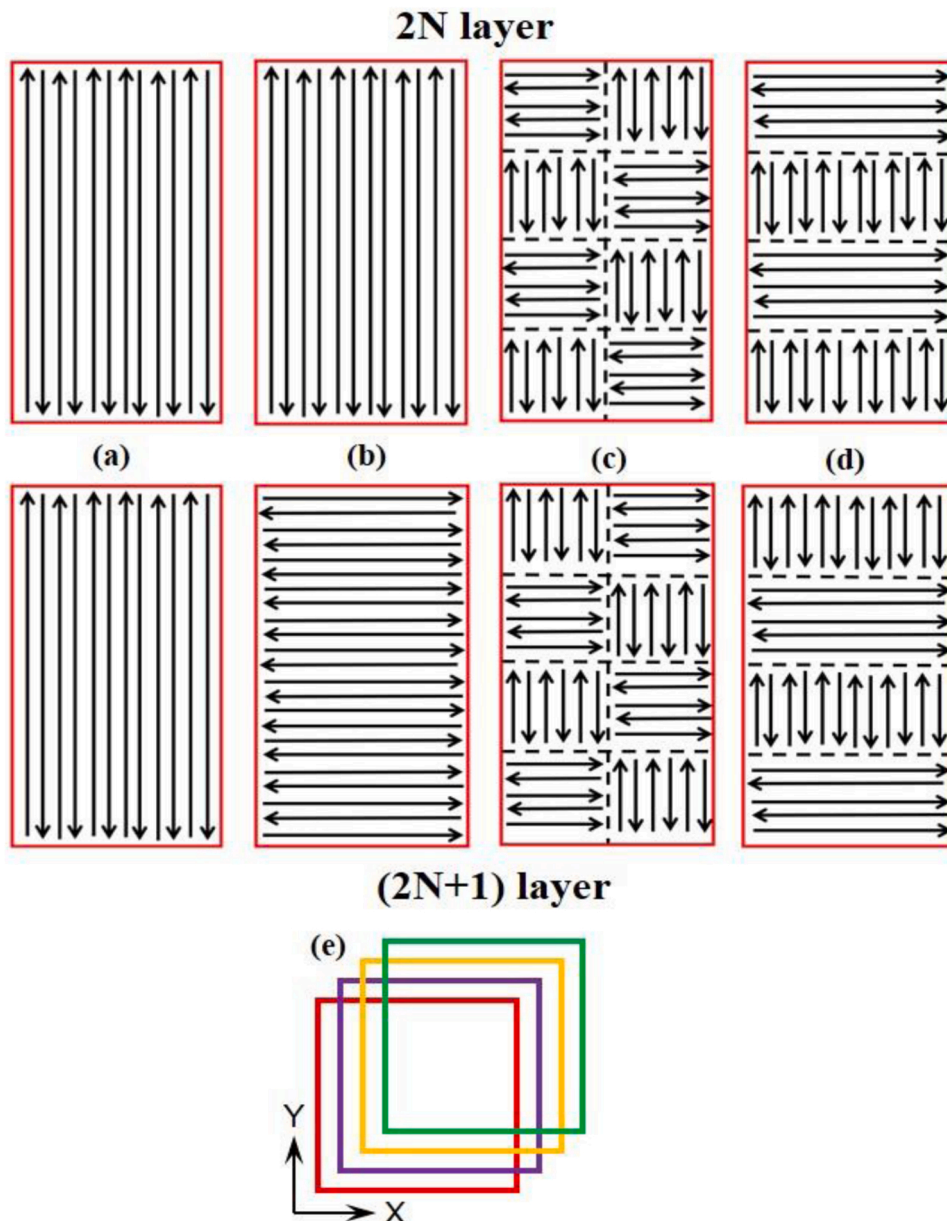

Fig. 1. Laser scanning patterns on subsequent layers under different scanning strategies, (a) unidirectional scanning, (b) bidirectional scanning, (c) island scanning; (d) chessboard scanning. In (e), a schematic of the shift between neighbouring layers.

2. Experimental approach

Gas-atomised Ti-6Al-4V powders in the size range of 20–50 μm were supplied by TLS Technik. A Concept Laser M2 Cusing SLM system, employing an Nd:YAG laser with a wavelength of 1075 nm and a maximum laser output power of 400 W (measured in continuous wave mode), was used to prepare 50 mm × 50 mm × 5 mm blocks of the material, with and without a base plate. Each block was produced with a different scanning strategy, including unidirectional, bidirectional, island scanning, and chessboard scanning. The details of the scanning patterns for each strategy on each layer are illustrated in Fig. 1. For the island scanning strategy, a cross section (or layer) is divided into a number of square islands, and the laser scanning direction within an island is perpendicular to those in the neighbouring islands. During processing, these "islands" are randomly scanned and the scan direction is rotated by 90° in a new layer. For all these scanning strategies, a shift along the X and Y directions by 1 mm in neighbouring layers, as shown in Fig. 1e, was used. The laser beam, with a spot size (d) of 75 μm in diameter, scanned the powders at a speed of 1000 mm/s. A hatch spacing (*i.e.*, the distance between two neighbouring hatch scan vectors) of $0.5d$ was adopted. The overlap of the scan vectors between two neighbouring islands was set to $0.15d$, while the overlap between the contour scan vector and the nearest raster scan vector is $0.25d$.

One block of as-built material with base plate from each scanning strategy was subjected to laser shock peening (LSP) post-manufacturing. The LSP was conducted on one of the 50 mm × 50 mm free surfaces of the as-built Ti-6Al-4V using a 10 GW/cm^2 laser with pulse duration of 18 ns. A square laser spot with a size of 3 mm × 3 mm was used. The material was covered with a black tape ablative layer and subject to double impacts adjusted for 50% overlap. Water was used as a plasma-confinement medium. The peening strategy adopted consisted in scanning the laser spot for patch-peening onto one of the free surfaces along the build direction (z-axis), as shown in Fig. 2a, with the laser hitting the material parallel to the y-axis. The as-built blocks with the base plates manufactured in each of the previously mentioned scanning strategies are illustrated in Fig. 2b.

Analyses of the surface profiles of the as-built blocks were carried out using a Bruker ContourGT-K0 3D optical scanning microscope. For each SLM scanning strategy, an area of 16 mm × 11 mm in the XY plane, perpendicular to the direction of material layer deposition, was surveyed.

Electron backscatter diffraction (EBSD) was used to investigate the grain orientation, using a Philips XL30 SEM, operated at 20 kV and with a 0.9 mm scanning step size. Samples were prepared by grinding with SiC paper and polishing down to sub-micron-size silica colloidal suspension. EBSD maps and pole figures on the XY or YZ-plane of selected samples were collected.

In order to evaluate the influence of the SLM scanning strategy, the use of base plate for layer deposition, and the post-manufacturing LSP process on the behaviour of the additively fabricated Ti-6Al-4V, residual stresses were characterised *via* the incremental hole drilling technique. Four 2-mm-diameter holes were drilled in each sample, along the y-direction, using a Stresscraft hole driller with the integral method of stress analysis, using the methodology recommended in the NPL Good Practice Guide (Grant et al., 2002). Strains were measured using a rosette strain gauge for hole drilling measurements, in a series of increasing increments as the hole depth increased, to an overall hole depth of 1.4 mm, in order to measure the σ_x and σ_z components of the residual stresses (XZ plane). The analysis provides the residual stress to a depth of 1 mm. The incremental hole drilling method has numerous sources of error, as discussed in the Good Practice Guide, that have been incorporated into estimates of inaccuracy on the data as presented here.

As will be described later in the Results section, the "worst" combination of manufacturing conditions was found to be the use of an island scanning strategy for SLM with a base plate. In consequence, a detailed TEM examination of the as-built and LSP-processed Ti-6Al-4V manufactured in these conditions was carried out. As-built island-scanned Ti-6Al-4V samples for TEM characterisation were extracted from different positions in the parent block and from the XZ plane of the LSP block, opposite to and at maximum distance from the peened surface. In the
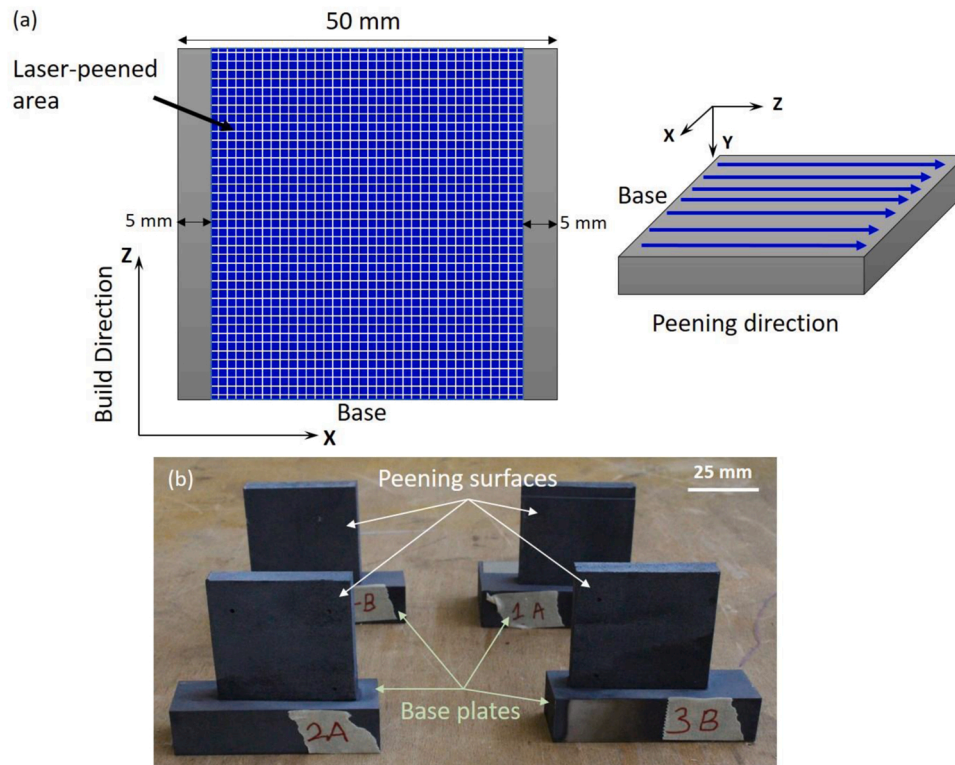

Fig. 2. (a) Schematic of the laser shock peening process and (b) additively manufactured Ti-6Al-4V blocks with an indication of the peened surfaces.

case of the LSP-processed material, samples for TEM were also extracted from the top (peened) surface down to 600 μm below it. In all cases, the slices were ground to approximately 90 μm thickness using 40 μm, 15 μm and 5 μm SiC paper grits, and cut into 3-mm-diameter discs. These latter were further thinned to electron beam transparency via jet electropolishing using a 5% perchloric acid (HClO₄) in ethanol solution at –50ºC as electrolyte. The examinations were conducted on a JEOL JEM 2100 transmission electron microscope operated at 200 kV in bright field (BF) imaging mode.

For quantitative TEM analysis, dislocation densities were calculated using a line intersection method, based on the superposition of a grid with a number of randomly oriented lines on the TEM micrographs. Each surveyed area of a foil was imaged under three or four different **g**-vectors, in order to check for dislocations that may not have been readily visible. Image-processing software was deployed for combining the resulting micrographs into an overlaid composite, on which a pattern of five lines with random orientations was drawn (Williams and Carter, 1996). An estimate of the uncertainties was made for the calculated dislocation density figures, taking into account variations in the foil thickness, errors in determining the angle between the zone axis and the plane of the defect (Fultz and Howe, 2012), and the underestimation associated with BF imaging mode, due to its incapacity of discriminating very close dislocations in a bundle (Norfleet et al., 2008). While other methods for estimating dislocation density are available, they are also affected by variations in the thickness of the examined foil (Klimiankou et al., 2005) and by distortions in its flatness in the region of analysis (Norfleet et al., 2008), offering similar uncertainty ranges. It is relevant to mention that, due to the nature of the aforementioned errors, the numbers hereby calculated serve as a lower bound for the dislocation densities.

3. Results

3.1. Structure of the material and residual stresses

The results from the 3D optical scanning microscopy of the surface profile of each block are presented in Fig. 3. A comparison between the topographic profiles indicates a higher degree of surface irregularity for the Ti-6Al-4V built using the island scanning strategy, whereas the chessboard-scanned as-built material provided the best surface profile amongst the investigated scanning strategies, with more uniformity in the layer deposition.

Fig. 4 summarises the observations from the EBSD survey on the as-built Ti-6Al-4V across several surveyed areas. The microstructure of the alloy consists of martensitic hcp α'-Ti laths and grains, and bcc prior-β grains, as shown in Fig. 4a. The martensitic hcp α'-phase has been identified, in EBSD, from the crystallographic relationships $(0001)_{\alpha'} \parallel (110)_\beta$ and $< 2\overline{1}\overline{1}0 >_{\alpha'} \parallel < 111 >_\beta$, and its presence is consistent with the high cooling rates due to SLM (Yan and Yu, 2015). The pole figures for the hcp α'-Ti and for the bcc β-Ti for each scanning strategy are shown in Fig. 4c. As can be seen, the unidirectional scanning promotes more pronounced orientation distribution for both phases. The bidirectional, island, and chess scans produced similar distributions of grain orientations in the microstructure. Two aspects, however, were common to all scanning strategies tested and are directly seen from Fig. 4c. One refers to the observation of a weak texture for the α'-Ti. The other, conversely, indicates a strong (100) texture for the retained columnar β grains, reported to develop along the grain growth direction (Simonelli et al., 2014).

Residual stresses along the z- and x-axis, determined from the surface of the material to 1000 μm of depth, are shown in Fig. 5a for the Ti-6Al-4V built on a base plate and Fig. 5b for the material built without a base plate. In practically all cases, the use of a base plate increased the magnitudes of the residual stresses present in the as-manufactured materials (the exception being the continuous unidirectional scanning strategy case). The support and restraints provided by the base plate promoted a nearly 200 MPa shift upwards in the σ_z components of the residual stresses and a 100 MPa shift in the σ_x components.

The residual stress profiles for the LSP-processed Ti-6Al-4V alloys produced with the island and continuous bidirectional scanning strategies are presented in Fig. 6. As can be seen, the peening process completely eliminated the high-magnitude tensile residual stresses in the material, introducing, instead, residual stresses of compressive nature in both analysed directions (z- and x-axis) up to ~1 mm from the reference surface.
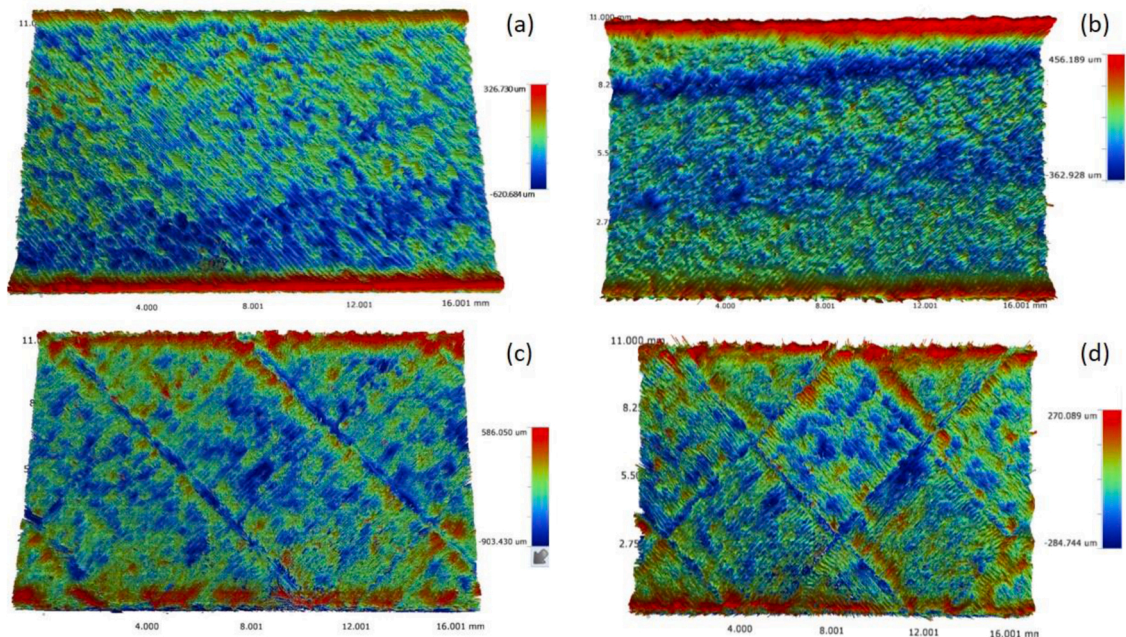

Fig. 3. 3D optical scanning surface profiles of the additively manufactured Ti-6Al-4V in different scanning strategies: (a) continuous unidirectional, (b) continuous bidirectional; (c) island and (d) chessboard. See Fig. 1 for the corresponding laser scanning schematics.
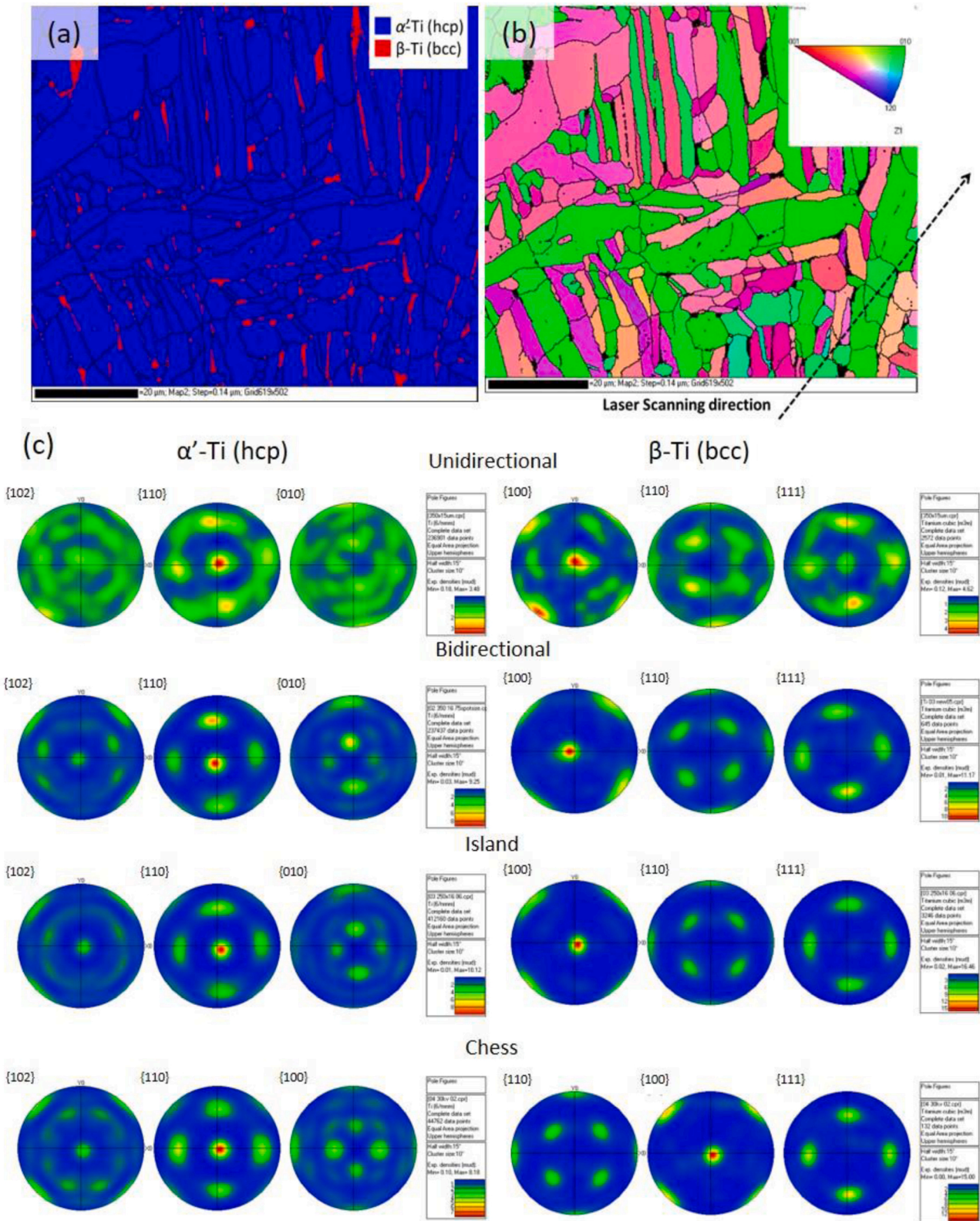
Fig. 4. EBSD map showing the grain morphology as well as the martensitic α'-phase and retained bcc β-Ti grains for the unidirectional scanned Ti-6Al-4V (a). The same map is presented in (b) with the IPF colour-coding identifying the orientation distribution and a line indicating the scanning direction. The pole figures for each phase in each scanned sample are seen in (c).

3.2. General TEM investigations

TEM analysis of the additively manufactured Ti-6Al-4V in island scanning strategy has shown significant differences between the as-built material and following LSP. As illustrated by Fig. 7, the as-built alloy displays signs of early deformation, with instances of wavy slip dislocations (tangles, junctions), predominance of loops and the presence of planar structures such as pile-ups and twins. These latter were observed
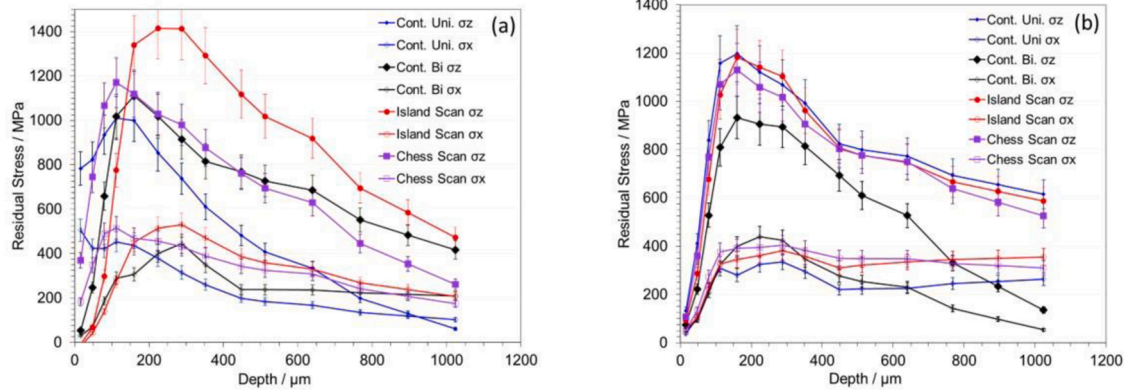
Fig. 5. Residual stresses as a function of distance from the surface in the as-built Ti-6Al-4V manufactured using a base plate (a) and manufactured without a base plate (b).
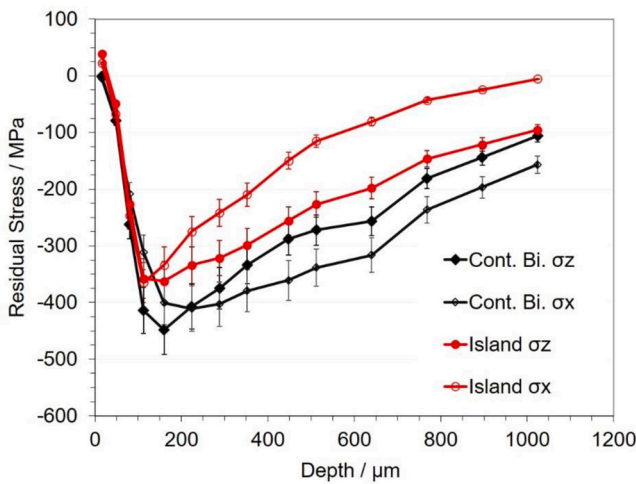

Fig. 6. Residual stress profiles as a function of depth in the laser-peened Ti-6Al-4V built with the continuous bidirectional and island scanning strategies.

in several micrographs, which revealed heavily twinned areas forming multidirectional intersections, such as the one shown in Fig. 7b.

The foils from the surface and subsurface regions of the built blocks where the laser shock peening process was carried out revealed a substantially different microstructure, in which more diverse dislocation arrangements were observed. Planar structures were still present, but now the most prominent of them are hexagonal networks. These hexagon-shaped structures are reported to result from the transformation of pile-ups, *via* the interaction of dislocation junctions, by lowering the Schmid factor associated with their glide planes (Feaugas, 1999; Fujita and Kimura, 1983), when more than one slip system is active. Fig. 8 illustrates these dislocation arrangements in the LSP Ti-6Al-4V microstructure for the surface foils (extracted between 0 and 300 µm) and for the subsurface foil (representing the material from depths 300–600 µm).

Wavy slip structures, such as multipoles, tangles, walls and cells, were prevalent in the LSP layers, whose observation revealed a more homogeneous distribution of dislocations within the grains than that of the as-built material. The micrographs in Fig. 9 depict the wavy slip dislocations along with a few planar structures, such as bowed dislocation lines. A relevant aspect of the LSP alloy images is that, despite the surveyed areas being more populated with dislocations, twins were much less observed in its microstructure.

For the as-built condition, the trace composites created from the TEM images for dislocation density estimates indicated a skewed, inhomogeneous distribution of dislocations and their structures, with areas less populated by dislocations in alternation with more strained regions. The average calculated density amounted to a minimum of 5.1×10^{13} m^{-2}. The same quantitative analysis applied to the LSP micrographs yielded a dislocation density of at least 1.1×10^{14} m^{-2}. A visual comparison of the results from the quantitative analysis of the Ti-6Al-4V, along with their uncertainties, is provided in Table 1. The much higher density found for the LSP processed material is explained on the basis that high-strain-rate plastic deformation is imparted to the matrix during peening, whereas the straining due to SLM is due to thermal effects, which is less effective than mechanical effects in promoting heavy dislocation-based substructures (Zhong et al., 2018).

3.3. Analysis of twins

Analyses of the TEM micrographs and their diffraction patterns indicate that the laser peening process altered the nature of the twins observed in the material. Fig. 10 shows a TEM micrograph of the as-built Ti-6Al-4V in which twins are detected. They have been identified as $\{10\bar{1}2\}$ from the positions of the reflexes in the selected-area electron diffraction pattern. This twin is very frequently observed in Ti-6Al-4V (Yang et al., 2016). The same procedure, applied to the LSP alloy, pointed to the presence of a different type of twins, found to belong to the $\{11\bar{2}2\}$ family, as illustrated by Fig. 11. In both cases, the twins were tens of nm wide and several hundreds of nm long, having a needle-like structure. Some twins, however, were a few hundreds of nm wide, presenting a lamellar aspect, as seen from Figs. 10a and 11a.

4. Discussion

The analyses of the surface profiles by 3D optical microscopy indicated that the surface quality of the additively manufactured alloy is sensitive to the scanning strategy. The chessboard layering produced a relatively smooth surface profile, while the unidirectional and bidirectional strategies yielded similar surfaces, and the island scanning resulted in topographic variations exceeding 1 mm.

Whilst the surface properties differed significantly as the strategy for layer deposition changed, the residual stress profiles were mainly similar. In all cases, the axial tensile residual stresses (σ_z component) developed during the SLM process reached peaks in excess of 1000 MPa, presenting magnitudes comparable to the reported yield strength of the alloy (Mertens et al., 2014; Rafi et al., 2013). The most deleterious combination of parameters for the SLM was the island scanning strategy with a base plate. As seen in Fig. 5a, the residual stress near the top surface of the as-built Ti-6Al-4V reached 1400 MPa, approaching the UTS of the additively manufactured material (Murr et al., 2009). These findings are surprising, considering that the island scanning pattern has been designed to reduce the levels of residual stress in as-built parts
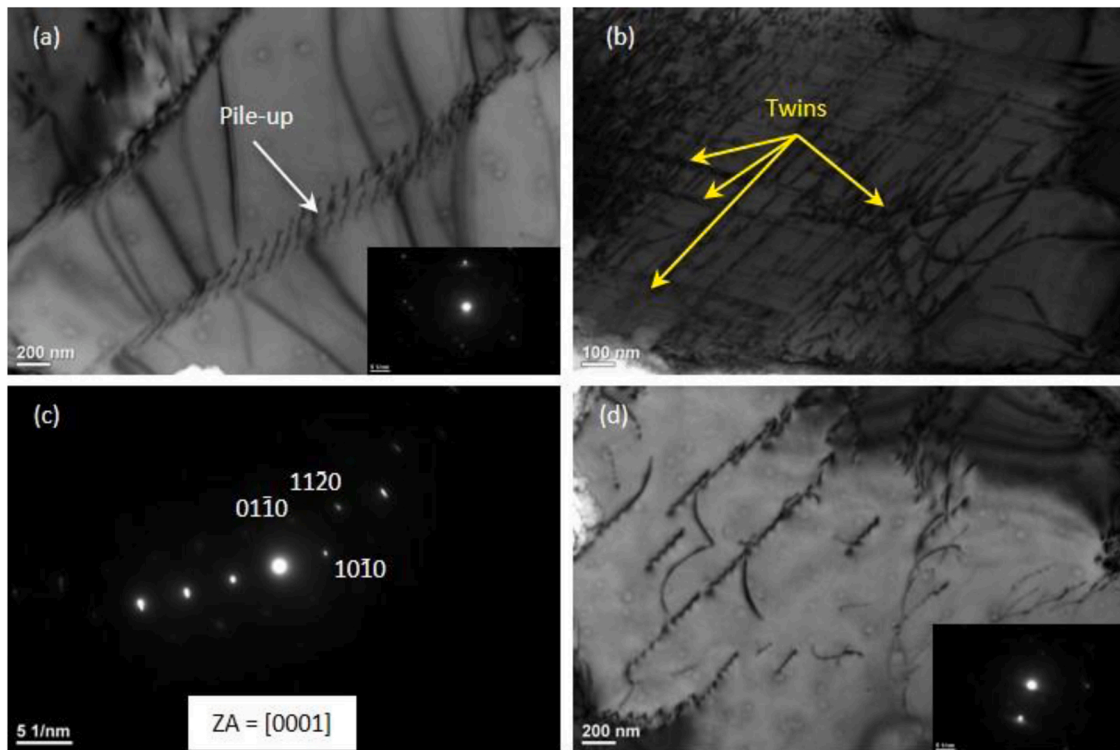
Fig. 7. Micrographs extracted from the surface (0–300 μm) of the parent as-built Ti-6Al-4V showing (a) a dislocation pile-up; (b) an area with multidirectional twin intersections (MTIs) observed from the basal plane, as indicated by the corresponding selected area diffraction pattern in (c); and some bowed dislocations forming loops and tangles in (d).
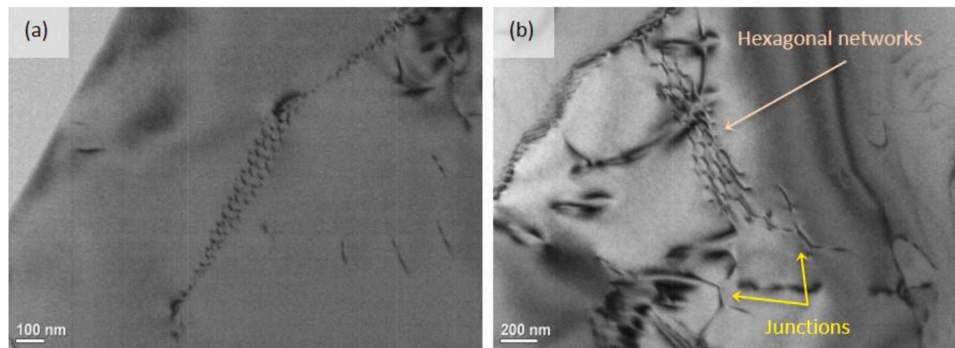

Fig. 8. A planar hexagonal network found on the surface (foils extracted between 0 and 300 μm) of the LSP Ti-6Al-4V material (a). In (b), the hexagonal network is accompanied by some attractive junctions, which indicate a transformation taking place in the subsurface material (300–600 μm depth).

(Sames et al., 2016), but are in agreement with previous investigations on materials manufactured by SLM (Wu et al., 2014). It must be noted that the effects of the scanning strategy on residual stress are not yet well understood, with a wide variety of residual stress levels being reported, depending on parameters such as scan vector length and rotation (Ali et al., 2018). The present study, though, suggests that the use of continuous scanning results in lower residual stress levels, behaviour also noted by Sames et al. (2016) and Wu et al. (2014). Another relevant aspect seen from Fig. 5 refers to the base plate, which seemed to intensify the development of axial residual stresses in the material built with the island scanning pattern, but had no significant effect for the other scanning strategies, nor on the transverse residual stress components. It is possible that, similarly to the scanning pattern, the presence (or not) of the base plate produces effects that are conditioned to many parameters, but this requires further examination.

Irrespective of the manufacturing conditions, the adoption of laser shock peening as a complementary process is noted as being potentially

desirable and advantageous. The pronounced temperature gradients experienced by the material during SLM (both melting and cooling) means tensile residual stresses will always be present in the as-built part. While methods aimed at reducing them in additively manufactured components are welcome, LSP is still a necessary step to transform tensile residual stress into compressive within hundreds of microns of depth. Its advantages are not limited to surface hardening, with recent works on Ti-6Al-4V evidencing both hardening of surface layers and grain refinement (Guo et al., 2018).

The EBSD microstructural analysis revealed features consistent with what is expected for Ti-6Al-4V produced by SLM. The parallelism relationships found in the survey indicated a fully martensitic hcp α'-Ti, a metastable phase associated with the fast cooling experienced by the alloy in SLM (Kazantseva et al., 2018), alongside bcc prior-β grains, whose vertical grain boundaries were detected by EBSD (Fig. 4a). Despite the crystallographic differences between the unidirectional scanned sample and its counterparts, all scanning strategies produced
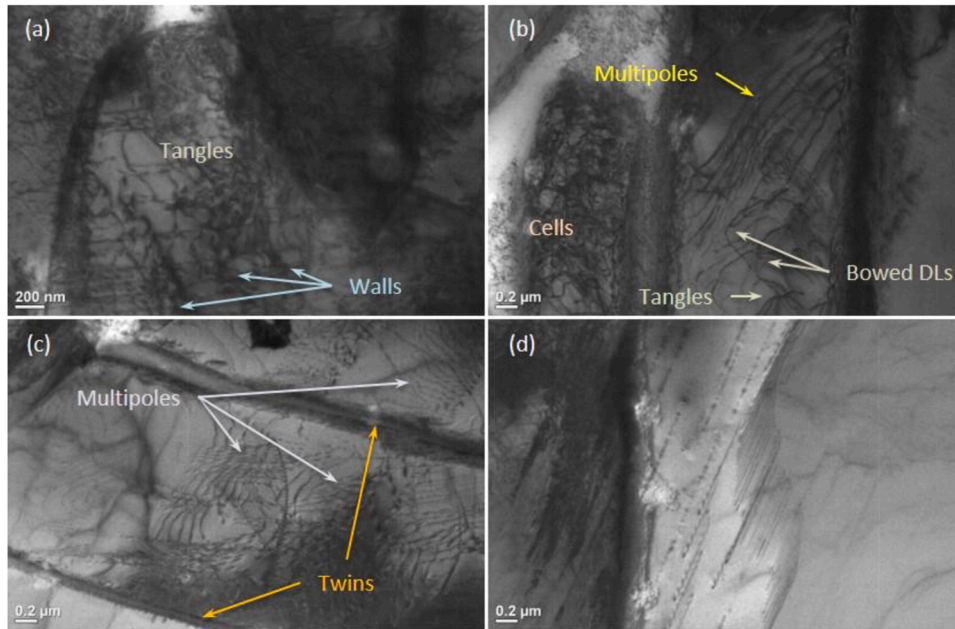
Fig. 9. Wavy slip dislocation arrangements depicted in the LSP material. The surface foils (extracted between 0 and 300 μm depth), illustrated in (a) and (b), showed a high density of dislocations, organised in poles, tangles, walls and cells. The subsurface foils (extracted between 300 and 600 μm depth) also revealed significant dislocation populations, with multipoles along several directions (c), and walls in a fairly parallel arrangement (d).

Table 1 –
Dislocation density obtained from the line intersection method and, in brackets, its uncertainty for each condition.

Condition	Average Dislocation Density / m^{-2}
LSP	1.1×10^{14} (4.0×10^{13})
As-built	5.1×10^{13} (2.2×10^{13})

weak α' texture, as seen in Fig. 4, from the multiple orientations of the martensitic grains formed within the prior-β phase. Likewise, the presence of the (100) pole in all β-Ti pole figures evidences epitaxial growth of the β grains, as successive layers are deposited, producing a strong texture along the grain growth direction and a columnar grain structure. These results are in agreement with those from similar investigations on SLM Ti-6Al-4V (Simonelli et al., 2014). Such findings suggest that the
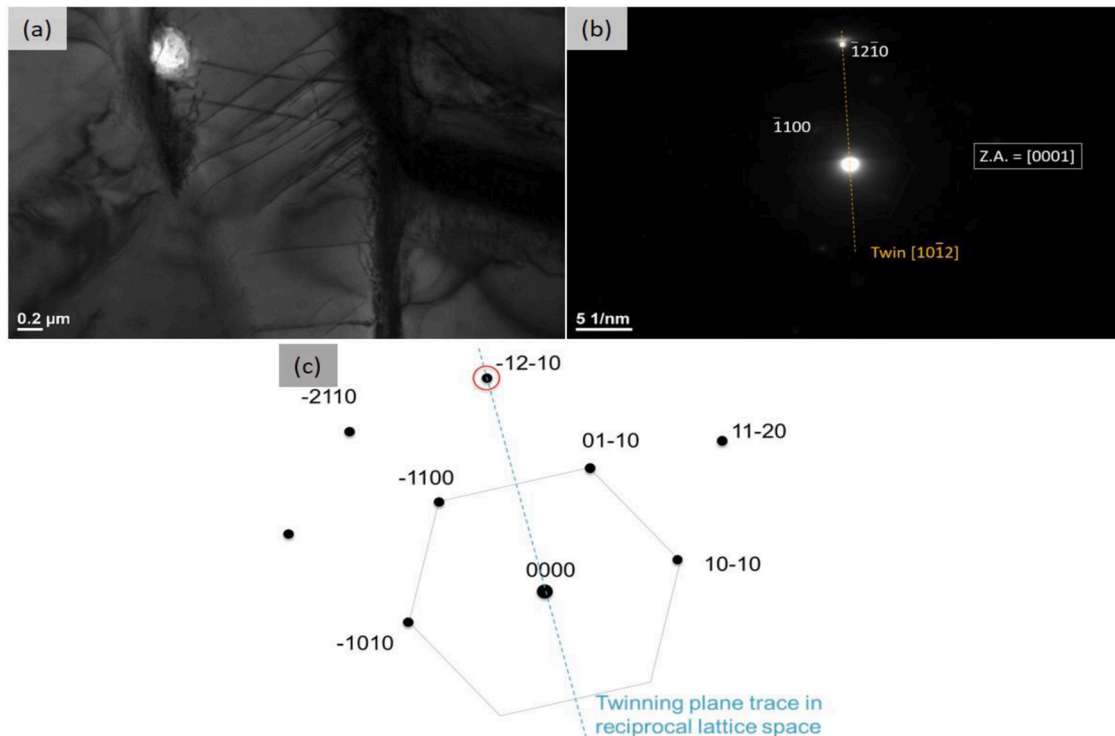

Fig. 10. Two-beam TEM micrograph of a subsurface (300–600 μm depth) layer of the as-built Ti-6Al-4V showing twins (a) and corresponding selected area diffraction pattern (b). A schema of the pattern showing the lattice symmetry plane of the twin is shown in (c).
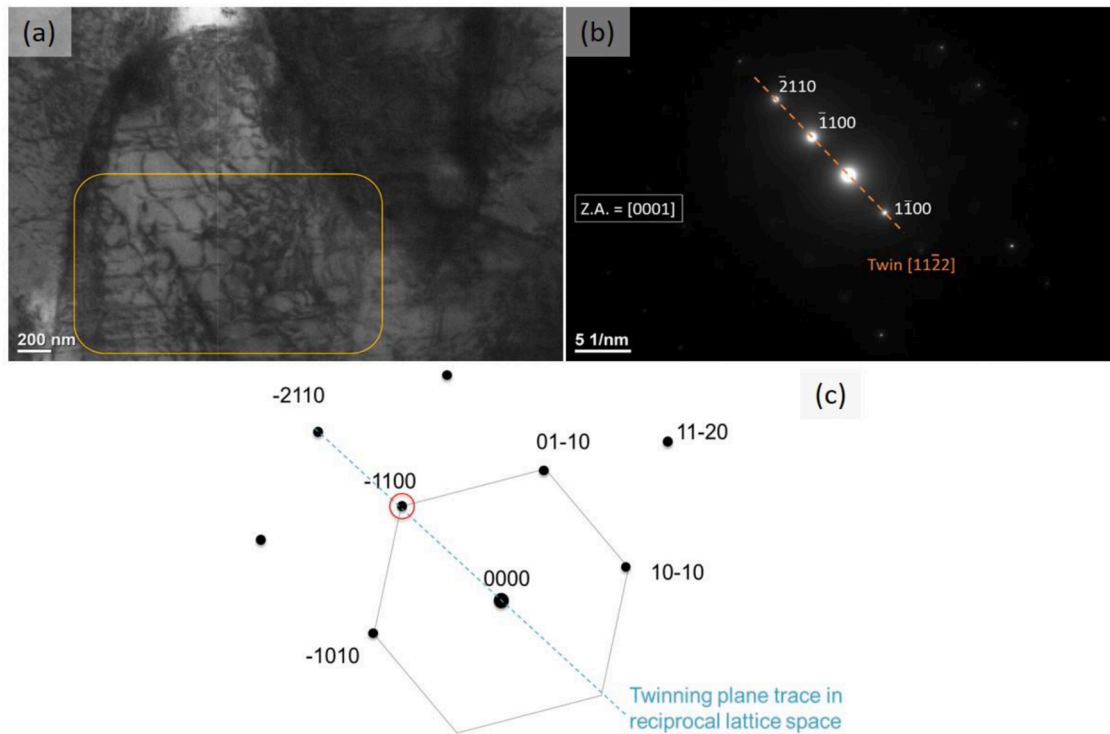
Fig. 11. Two-beam micrograph of a subsurface (300–600 μm depth) sample of the LSP Ti-6Al-4V in (a), showing a few twins identified in the SAED as {11$\overline{2}$2} (b). A schema of the diffraction pattern is presented in (c).

scanning strategy does not exercise a significant effect on the grain morphology and orientation.

The TEM study indicates some straining experienced by the alloy during SLM, related to the severe thermal history; and a strongly deformed microstructure following LSP, as the magnitudes of the dislocation densities in Table 1 show. However, the most significant aspect of the TEM survey relates to twinning: that is, twinning is abundant in the as-built Ti-6Al-4V and significantly reduced following LSP. The presence of twins in the microstructure of the as-built alloy is not a surprising result. Krakhmalev et al. (2016) attributed the development in the microstructure of the SLM Ti-6Al-4V to the thermal stresses induced by the thermal gradients, prompting the emergence of a strain accommodation mechanism. Considering that the *hcp* structure has a limited number of independent slip systems for dislocation motion (Liu et al., 2013), it is reasonable that the current work identified areas with large quantities of twins in the as-built alloy, required to ensure deformation compatibility out of the basal and prismatic planes, along the c-axis of the hexagonal lattice (Chichili et al., 1998; Sun et al., 2013).

In the case of the LSP-processed Ti-6Al-4V, a variety of results were reported, with contradictory accounts. Lainé et al. (2017) reported twins to be practically absent from the microstructure of their conventionally manufactured alloy following LSP; evidences of twins are also not found in the investigation conducted by Lu et al. (2016) on Ti-6Al-4V manufactured by selective electron beam melting process, from the powder bed fusion route. Other studies on both conventional (Ren et al., 2016) and additively manufactured (Guo et al., 2018) Ti-6Al-4V showed abundant thin, needle-shaped twins in the microstructure. In some cases, depending on the number of impacts and on the laser pulse energy, these twins even formed the same multidirectional twin intersections (MTIs) observed in Fig. 7b. The present work seemed, at first, to support the idea of few (or absent) twins, given that instances of twinned planes were much less often observed in the LSP micrographs. However, an analysis of the role of each microstructural feature highlighted by the TEM examination reveals that the presence of twins is possible and that, in reality, no contradiction exists. The dislocation

structures found in the as-built material range from pile-ups to multi-directional twin intersections (MTIs), a result that indicates that one or, at most, two slip systems were active during the SLM-induced deformation. Even if more systems were active, twinning would still occur, given that only four independent slip systems exist for the *hcp* structure, while a minimum of five is required to maintain plastic deformation compatibility in polycrystalline materials (Wu et al., 2011). Given that the most significant effect of twinning is to reorient portions of the crystal to positions that are more favourable to slip, it becomes reasonable to admit that heavily twinned areas, with a high density of MTIs, will favour dislocation generation and motion, rather than further twinning, if further deformation is induced. Thus, the LSP process, when applied to an as-built material in similar conditions to that in Fig. 7, which is already considerably twinned, would trigger intense plastic deformation by slip, causing early dislocation arrangements to evolve into walls, cells and others while suppressing the formation of twins. This explains the much higher dislocation density found for the LSP alloy, in comparison to the as-built counterpart. And, since the evolution of the dislocation structures depends on the pre-LSP condition of the material (grain size, deformation level) and on the LSP parameters (energy, number of impacts, induced strain rate), it is not surprising that a wide variety of post-processing microstructures are observed, some densely populated by twins, some containing very few instances – or even devoid of them. Irrespective of the case, in the event of continued straining, dislocation slip will always follow the onset of twinning, since this mechanism cannot accommodate large deformations in the lattice due to the fact that atom displacements are much less than the inter-atomic distance (Wen et al., 2009).

The qualitative TEM investigation provides a complementary perspective on the analysis of twinning in Ti-6Al-4V. The predominant twin type found in the as-built material was the {10$\overline{1}$2}⟨$\overline{1}$011⟩, known to be generated by tensile straining in titanium (Wang et al., 2010; Wielewski et al., 2012). This correlates well with the high-magnitude tensile residual stresses shown in Fig. 5 of the present study, and with the findings of Xiao et al. (2020) and Yadroitsev and Yadroitsava (2015),

who also measured residual stresses in Ti-6Al-4V manufactured by SLM. Also, the presence of tensile twins in the substructure is associated with the existence of preceding high-magnitude compressive stresses (Kazantseva et al., 2018), developed in the material during the building process by deposition of sequential layers. As for the LSP alloy, its less frequently observed twins were found to be of the $\{11\bar{2}2\}\langle11\bar{2}3\rangle$ type. Once again, agreement with the nature of the residual stresses in the material is noticed, since this twinning system is compressive. However, this system was not initially expected, considering that the $\{10\bar{1}1\}\langle10\bar{1}2\rangle$ variant of compressive twin, with half the shear strain of the $\{11\bar{2}2\}\langle11\bar{2}3\rangle$ twin, is available for *hcp* metals (Christian and Mahajan, 1995). The predominance of the $\{11\bar{2}2\}$ can be rationalised by considering that the preferred twin system in a given material depends on several parameters such as the critical resolved shear stress (CRSS), strain level, and texture. As an example of this, Sun et al. (2013) also identified the $\{11\bar{2}2\}$ twin system as the predominant compression twin, along with the tensile $\{10\bar{1}2\}$, in ultrafine-grained Ti processed by dynamic plastic deformation. It is suggested that $\{11\bar{2}2\}$ twinning is favoured when the [0001] direction of the metallic matrix is nearly parallel to the loading direction (Munroe et al., 1997). Irrespective of the type, the predominance of compressive twins in the substructure of the LSP Ti-6Al-4V is reasonable, given that these twins are formed when a compressive force is applied along the *c* axis of the hcp structure, which may have been the case during peening.

Both quantitative and qualitative TEM analyses converge to indicate that twinning has a significant role in ensuring continuity and compatibility of deformation in any transformation the microstructure of the material may suffer as a result of its processing. Thus, it is expected that deformation in Ti-6Al-4V proceeds by alternating dislocation slip and twinning.

5. Conclusions

The present study has demonstrated that:

1. Amongst the four scanning strategies adopted for SLM of Ti-6Al-4V, the island pattern is shown to be the most deleterious, in terms of more pronounced surface irregularity and the highest level of tensile residual stress, particularly when a base plate (or substrate) is used. In contrast, the continuous scanning strategies were noted to lower the peak residual stresses, and the chessboard scan produced a smoother surface.
2. The scanning strategy adopted does not affect the microstructure of the SLM Ti-6Al-4V, given that all patterns adopted produced similar grain orientation distributions, with weak texture for the martensitic α' phase and a strong (100) texture for the columnar β grains.
3. High-magnitude tensile residual stresses resulted from the SLM process, with the stress component in the build direction (z-axis) being comparable to the material's yield stress. LSP successfully eliminates the tensile residual stress, introducing compressive residual stresses to a depth of several hundreds of microns from the surface.
4. The dislocation density of the LSP material is significantly higher than that of the as-built, indicating intense plastic deformation during the peening process. However, after the LSP processing, twins are noted to play an important role in assuring deformation compatibility, allowing dislocation generation and motion to occur in the *hcp* structure.
5. The substructure of the as-built Ti-6Al-4V showed a predominance of early dislocation arrangements such as pile-ups along with a high density of twins. Wavy slip structures such as bowed dislocation lines, loops and tangles were also found. The LSP Ti-6Al-4V presented a more diverse range of substructural features, with predominance of wavy slip structures (multipoles, walls and cells),

along with remnants of planar arrangements such as junctions and networks. Also, fewer instances of twins were observed.
6. The $\{10\bar{1}2\}$ tensile twinning system predominated in the as-built substructure, while $\{11\bar{2}2\}$ compressive twins were the prevalent type in the LSP alloy matrix. In both cases, the twinning system correlated to the nature of the detected residual stresses in the material.

CRediT authorship contribution statement

José Rodolpho de Oliveira Leo: Conceptualization, Investigation, Writing – original draft. **Suraiya Zabeen:** Methodology, Project administration, Visualization. **Michael E. Fiztpatrick:** Funding acquisition, Supervision, Writing – review & editing. **Ji Zou:** Investigation, Validation. **Moataz M. Attallah:** Data curation, Supervision.

Declaration of Competing Interest

The authors declare that they have no known competing financial interests or personal relationships that could have appeared to influence the work reported in this paper.

Data availability

Data will be made available on request.

Acknowledgements

References

Ali, H., Ghadbeigi, H., Mumtaz, K., 2018. Effect of scanning strategies on residual stress and mechanical properties of Selective Laser Melted Ti6Al4V. Mater. Sci. Eng. A 712 (December 2017), 175–187. https://doi.org/10.1016/j.msea.2017.11.103.

Bhadeshia, H.K.D.H., n.d., Titanium & its Alloys (pp. 1–13). pp. 1–13. Retrieved from http://www.msm.cam.ac.uk/phase-trans/2000/C9/lecture3.pdf.

Boyer, R.R., 1996. An overview on the use of titanium in the aerospace industry. Mater. Sci. Eng. A 213 (1–2), 103–114. https://doi.org/10.1016/0921-5093(96)10233-1.

Chichili, D.R., Ramesh, K.T., Hemker, K.J., 1998. The high-strain-rate response of alpha-titanium: Experiments, deformation mechanisms and modeling. Acta Mater. 46 (3), 1025–1043. https://doi.org/10.1016/S1359-6454(97)00287-5.

Christian, J.W., Mahajan, S., 1995. Deformation twinning. Prog. Mater. Sci. 39 (1–2), 1–157. https://doi.org/10.1016/0079-6425(94)00007-7.

Feaugas, X., 1999. On the origin of the tensile flow stress in the stainless steel AISI 316L at 300 K: back stress and effective stress. Acta Mater. 47 (13), 3617–3632. https://doi.org/10.1016/S1359-6454(99)00222-0.

Fujita, H., Kimura, S., 1983. Role of Conjugate Slip in Deformation of Cu-10%Al Single Crystals. J. Phys. Soc. Jpn. 52 (1), 157–167.

Fultz, B., Howe, J., 2012. Transmission Electron Microscopy and Diffractometry of Materials, 4th ed.,. Springer,.

Grant, P.V., Lord, J.D., Whitehead, P.S., 2002. The Measurement of Residual Stresses by the Incremental Hole Drilling Technique. In: Measurement Good Practice Guide, No. 53. Teddington, UK: National Physical Laboratory,, p. 44.

Guo, W., Sun, R., Song, B., Zhu, Y., Li, F., Che, Z., Peng, P., 2018. Laser shock peening of laser additive manufactured Ti6Al4V titanium alloy. Surf. Coat. Technol. 349 (February), 503–510. https://doi.org/10.1016/j.surfcoat.2018.06.020.

Kalentics, N., Huang, K., Ortega Varela de Seijas, M., Burn, A., Romano, V., Logé, R.E., 2019. Laser shock peening: A promising tool for tailoring metallic microstructures in selective laser melting. J. Mater. Process. Technol. 266 (November 2018), 612–618. https://doi.org/10.1016/j.jmatprotec.2018.11.024.

Kasperovich, G., Hausmann, J., 2015. Improvement of fatigue resistance and ductility of selective laser molten TiAl6V4. J. Mater. Process. Technol. 220 (220), 202–214. https://doi.org/10.1016/j.jmatprotec.2015.01.025ISBNISSN:0924-0136ISSN0924-0136.

Kazantseva, N., Krakhmalev, P., Thuvander, M., Yadroitsev, I., Vinogradova, N., Ezhov, I., 2018. Martensitic transformations in Ti-6Al-4V (ELI) alloy manufactured by 3D Printing. Mater. Charact. 146 (July), 101–112. https://doi.org/10.1016/j.matchar.2018.09.042.

Klimiankou, M., Lindau, R., Möslang, A., 2005. Energy-filtered TEM imaging and EELS study of ODS particles and argon-filled cavities in ferritic-martensitic steels. Micron (Oxf., Engl.: 1993) 36 (1), 1–8. https://doi.org/10.1016/j.micron.2004.08.001.

Krakhmalev, P., Fredriksson, G., Yadroitsava, I., Kazantseva, N., Du Plessis, A., Yadroitsev, I., 2016. Deformation behavior and microstructure of Ti6Al4V manufactured by SLM. Phys. Procedia 83, 778–788. https://doi.org/10.1016/j.phpro.2016.08.080.

Lainé, S.J., Knowles, K.M., Doorbar, P.J., Cutts, R.D., Rugg, D., 2017. Microstructural characterisation of metallic shot peened and laser shock peened Ti–6Al–4V. Acta Mater. 123, 350–361. https://doi.org/10.1016/j.actamat.2016.10.044.

Lan, L., Xin, R., Jin, X., Gao, S., He, B., Rong, Y., Min, N., 2020. Effects of laser shock peening on microstructure and properties of Ti-6Al-4V titanium alloy fabricated via selective laser melting. Materials 13 (15), 1–11. https://doi.org/10.3390/MA13153261.

Liu, H.X., Hu, Y., Wang, X., Shen, Z.B., Li, P., Gu, C.X., Guo, C., 2013. Grain refinement progress of pure titanium during laser shock forming (LSF) and mechanical property characterizations with nanoindentation. Mater. Sci. Eng. A 564, 13–21. https://doi.org/10.1016/j.msea.2012.11.087.

Liu, S., Shin, Y.C., 2019. Additive manufacturing of Ti6Al4V alloy: A review. Mater. Des. 164, 107552 https://doi.org/10.1016/j.matdes.2018.107552.

Lu, J., Lu, H., Xu, X., Yao, J., Cai, J., Luo, K., 2020. High-performance integrated additive manufacturing with laser shock peening –induced microstructural evolution and improvement in mechanical properties of Ti6Al4V alloy components. Int. J. Mach. Tools Manuf. 148 (October 2019), 103475 https://doi.org/10.1016/j.ijmachtools.2019.103475.

Lu, S.L., Qian, M., Tang, H.P., Yan, M., Wang, J., StJohn, D.H., 2016. Massive transformation in Ti-6Al-4V additively manufactured by selective electron beam melting. Acta Mater. 104, 303–311. https://doi.org/10.1016/j.actamat.2015.11.011.

Mertens, A., Reginster, S., Paydas, H., Contrepois, Q., Dormal, T., Lemaire, O., Lecomte-Beckers, J., 2014. Mechanical properties of alloy Ti–6Al–4V and of stainless steel 316L processed by selective laser melting: influence of out-of-equilibrium microstructures. Powder Metall. 57 (3), 184–189. https://doi.org/10.1179/1743290114Y.0000000092.

Munroe, N., Tan, X., Gu, H., 1997. Orientation dependence of slip and twinning in HCP metals. Scr. Mater. 36 (12), 1383–1386. https://doi.org/10.1016/S1359-6462(97)00048-1.

Murr, L.E., Quinones, S.A., Gaytan, S.M., Lopez, M.I., Rodela, A., Martinez, E.Y., Wicker, R.B., 2009. Microstructure and mechanical behavior of Ti-6Al-4V produced by rapid-layer manufacturing, for biomedical applications. J. Mech. Behav. Biomed. Mater. 2 (1), 20–32. https://doi.org/10.1016/j.jmbbm.2008.05.004.

Nie, X., He, W., Zhou, L., Li, Q., Wang, X., 2014. Experiment investigation of laser shock peening on TC6 titanium alloy to improve high cycle fatigue performance. Mater. Sci. Eng. A 594, 161–167. https://doi.org/10.1016/j.msea.2013.11.073.

Norfleet, D.M., Dimiduk, D.M., Polasik, S.J., Uchic, M.D., Mills, M.J., 2008. Dislocation structures and their relationship to strength in deformed nickel microcrystals. Acta Mater. 56 (13), 2988–3001. https://doi.org/10.1016/j.actamat.2008.02.046.

Parry, L., Ashcroft, I.A., Wildman, R.D., 2016. Understanding the effect of laser scan strategy on residual stress in selective laser melting through thermo-mechanical simulation. Addit. Manuf. 12, 1–15. https://doi.org/10.1016/j.addma.2016.05.014.

Qiu, C., Adkins, N.J.E., Attallah, M.M., 2013. Microstructure and tensile properties of selectively laser-melted and of HIPed laser-melted Ti-6Al-4V. Mater. Sci. Eng. A 578, 230–239. https://doi.org/10.1016/j.msea.2013.04.099.

Rafi, H.K., Karthik, N.V., Gong, H., Starr, T.L., Stucker, B.E., 2013. Microstructures and Mechanical Properties of Ti6Al4V Parts Fabricated by Selective Laser Melting and Electron Beam Melting. J. Mater. Eng. Perform. 22 (12), 3872–3883. https://doi.org/10.1007/s11665-013-0658-0.

Ren, X.D., Zhou, W.F., Liu, F.F., Ren, Y.P., Yuan, S.Q., Ren, N.F., Yang, T., 2016. Microstructure evolution and grain refinement of Ti-6Al-4V alloy by laser shock

processing. Appl. Surf. Sci. 363, 44–49. https://doi.org/10.1016/j.apsusc.2015.11.192.

Sames, W.J., List, F.A., Pannala, S., Dehoff, R.R., Babu, S.S., 2016. The metallurgy and processing science of metal additive manufacturing. Int. Mater. Rev. 61 (5), 315–360. https://doi.org/10.1080/09506608.2015.1116649.

Simonelli, M., Tse, Y.Y., Tuck, C., 2014. Effect of the build orientation on the mechanical properties and fracture modes of SLM Ti-6Al-4V. Mater. Sci. Eng. A 616, 1–11. https://doi.org/10.1016/j.msea.2014.07.086.

Simonelli, Marco, Tse, Y.Y., Tuck, C., 2014. On the Texture Formation of Selective Laser Melted Ti-6Al-4V. Metall. Mater. Trans. A 45 (6), 2863–2872. https://doi.org/10.1007/s11661-014-2218-0.

Sun, J.L., Trimby, P.W., Si, X., Liao, X.Z., Tao, N.R., Wang, J.T., 2013. Nano twins in ultrafine-grained Ti processed by dynamic plastic deformation. Scr. Mater. 68 (7), 475–478. https://doi.org/10.1016/j.scriptamat.2012.11.025.

Thijs, L., Verhaeghe, F., Craeghs, T., Humbeeck, J., Van Kruth, J.P., 2010. A study of the microstructural evolution during selective laser melting of Ti-6Al4V. Acta Mater. 58 (9), 3303–3312. https://doi.org/10.1016/j.actamat.2010.02.004.

Vrancken, B., Thijs, L., Kruth, J.P., Van Humbeeck, J., 2012. Heat treatment of Ti6Al4V produced by Selective Laser Melting: Microstructure and mechanical properties. J. Alloy. Compd. 541, 177–185. https://doi.org/10.1016/j.jallcom.2012.07.022.

Wang, L., Yang, Y., Eisenlohr, P., Bieler, T.R., Crimp, M.A., Mason, D.E., 2010. Twin nucleation by slip transfer across grain boundaries in commercial purity titanium. Metall. Mater. Trans. A: Phys. Metall. Mater. Sci. 41 (2), 421–430. https://doi.org/10.1007/s11661-009-0097-6.

Wen, M., Liu, G., Gu, J. feng, Guan, W. ming, Lu, J., 2009. Dislocation evolution in titanium during surface severe plastic deformation. Appl. Surf. Sci. 255 (12), 6097–6102. https://doi.org/10.1016/j.apsusc.2009.01.048.

Wielewski, E., Siviour, C.R., Petrinic, N., 2012. On the correlation between macrozones and twinning in Ti-6Al-4V at very high strain rates. Scr. Mater. 67 (3), 229–232. https://doi.org/10.1016/j.scriptamat.2012.04.026.

Williams, D.B., Carter, C.B., 1996. Transmission Electron Microscopy: A Textbook for Materials Science, 1st ed.,. Springer,.

Wu, A.S., Brown, D.W., Kumar, M., Gallegos, G.F., King, W.E., 2014. An Experimental Investigation into Additive Manufacturing-Induced Residual Stresses in 316L Stainless Steel. Metall. Mater. Trans. A 45 (13), 6260–6270. https://doi.org/10.1007/s11661-014-2549-x.

Wu, X.L., Youssef, K.M., Koch, C.C., Mathaudhu, S.N., Kecskés, L.J., Zhu, Y.T., 2011. Deformation twinning in a nanocrystalline hcp Mg alloy. Scr. Mater. 64 (3), 213–216. https://doi.org/10.1016/j.scriptamat.2010.10.024.

Xiao, Z., Chen, C., Zhu, H., Hu, Z., Nagarajan, B., Guo, L., Zeng, X., 2020. Study of residual stress in selective laser melting of Ti6Al4V. Mater. Des. 193, 108846 https://doi.org/10.1016/j.matdes.2020.108846.

Yadroitsev, I., Yadroitsava, I., 2015. Evaluation of residual stress in stainless steel 316L and Ti6Al4V samples produced by selective laser melting. Virtual Phys. Prototyp. 10 (2), 67–76. https://doi.org/10.1080/17452759.2015.1026045.

Yan, M., Yu, P., 2015. An Overview of Densification, Microstructure and Mechanical Property of Additively Manufactured Ti-6Al-4V — Comparison among Selective Laser Melting, Electron Beam Melting, Laser Metal Deposition and Selective Laser Sintering, and with Conventional Po. In: Lakshmana, A. (Ed.), Sintering Techniques of Materials, pp. 77–106. https://doi.org/10.5772/59275.

Yang, J., Yu, H., Yin, J., Gao, M., Wang, Z., Zeng, X., 2016. Formation and control of martensite in Ti-6Al-4V alloy produced by selective laser melting. Mater. Des. 108, 308–318. https://doi.org/10.1016/j.matdes.2016.06.117.

Zhong, H.Z., Zhang, X.Y., Wang, S.X., Gu, J.F., 2018. Examination of the twinning activity in additively manufactured Ti-6Al-4V. Mater. Des. 144, 14–24. https://doi.org/10.1016/j.matdes.2018.02.015.